UVRR Spectroscopy and Vibrational Analysis of Mercury Thiolate Compounds Resembling d^{10} Metal Binding Sites in Proteins

Gerhard Fleissner,[†] Pawel M. Kozlowski,[†] Mária Vargek,[†] James W. Bryson,[‡] Thomas V. O'Halloran,[‡] and Thomas G. Spiro*,[†]

Department of Chemistry, Princeton University, Princeton, New Jersey 08544, Department of Chemistry and Department of Biochemistry, Molecular Biology, and Cellular Biology, Northwestern University, Evanston, Illinois 60208

Received August 27, 1998

Raman, ultraviolet resonance Raman (UVRR) and far-IR spectra are reported for the mercury-cysteamine complex, $Hg(SCH_2CH_2NH_2)_2$. Band assignments are made for $Hg(SCH_2CH_2NH_2)_2$, and also for $[Hg(SBu^t)_3]^-$ and $[Hg(SMe)_3]^-$ on the basis of ab initio calculations with the effective core potential approximation and also on the basis of comparison with vibrational data of corresponding thiols. The calculations show that geometry-optimized $[Hg(SBu^t)_3]^-$ and $[Hg(SMe)_3]^-$ have virtually the same Hg−S bond lengths, but very different ν_s HgS frequencies, 196 and 268 cm^{-1}, in good agreement with the experimental data. The exceptionally low HgS frequency for $[Hg(SBu^t)_3]^-$ compared to $[Hg(SMe)_3]^-$ and to the Hg-MerR protein results from kinematic interactions of the Hg−S stretching and S−C−C bending coordinates when all three substituents at C_α are carbon atoms. For $Hg(SCH_2CH_2NH_2)_2$, the HgS stretching coordinate is distributed over three modes, at 339, 273, and 217 cm^{-1}, all of which exhibit UVRR enhancement. The other contributors to these modes are angle bending and torsional coordinates of the chelate rings. Involvement of the CCN bending coordinates is supported by observed and calculated frequency shifts in D_2O. The excitation profiles track the main UV absorption band, associated with S→Hg charge transfer. Enhancement is attributable to the weakening of the Hg−S bonds in the excited state, and probably to changes in the SCC bond angle. Also enhanced, albeit weakly, is the ν_{CS} mode at 658 cm^{-1}, reflecting C−S bond shortening in the excited state. The mingling of metal-sulfur and internal ligand coordinates is reminiscent of the mingling seen in RR spectra of type 1 Cu proteins. In both cases the phenomenon may be associated with elevated torsional contributions associated with the rigidity of the ligands.

Introduction

Proteins containing d^{10} metals play prominent roles in biology but have few spectroscopic handles, because of their closed shell electronic structure. They are silent to EPR spectroscopy and have no visible electronic transitions. They do, however, have $RS^- \rightarrow M$ charge transfer (CT) transitions which give rise to strong absorption in the 230−300 nm region, when, as is often the case, one or more of the protein ligands are cysteine side chains. We have recently shown[1] that it is possible to use ligand to metal charge transfer (LMCT) transitions of d^{10} metals bound to cysteinate ligands in a Hg-binding protein for generating resonance enhanced Raman bands with UV excitation.

To use ultraviolet resonance Raman (UVRR) spectroscopy as a tool for obtaining information on the metal coordination it is necessary to understand the vibrational patterns of d^{10} metal sulfur compounds, particularly the different factors influencing metal−ligand modes. In this study we present a vibrational analysis of the 3-coordinate aliphatic Hg−S compounds, $[Hg(SBu^t)_3]^-$ and $[Hg(SMe)_3]^-$, which possess essentially the same Hg coordination as proposed for the metal receptor site in the Hg-MerR metalloregulatory protein, a heavy metal receptor component of an Hg(II)-responsive genetic switch.[2] In addition, vibrational data including UVRR spectra and band assignments are presented for the cysteamine complex $Hg(SCH_2CH_2NH_2)_2$. This complex bears a structural resemblance to type 1 copper proteins[3]; the metal is bound to two S- and two N-ligands in a tetrahedral fashion.[4] The Hg−S bond lengths, 2.36 Å, are close to the Hg−S[cys] bond length in Hg-plastocyanin, 2.38 Å,[3] and furthermore the same C_α substitution pattern is present as in the cysteine ligand of the protein. Spectral features obtained for $Hg(SCH_2CH_2NH_2)_2$ may be useful for future UVRR spectroscopic studies on d^{10} metal type 1 copper proteins.

Experimental Section

Bis(2-aminoethanethiolate)mercury(II), $Hg(SCH_2CH_2NH_2)_2$, was prepared[4] by combining $HSCH_2CH_2NH_2 \cdot HCl$ (1.14 g, 10 mmol), HgO (1.08 g, 5 mmol), and tetramethylammonium hydroxide (4.2 mL 25% in MeOH, 10 mmol) in 20 mL of absolute ethanol and stirring at 50 °C for 2 h. The solution was allowed to cool slowly to room temperature and was then stored overnight at −4 °C. Small crystalline plates were collected by vacuum filtration, washed with cold ethanol followed by diethyl ether, and dried in vacuo. Yield 1.1 g (62%), mp 86.2−87.5 °C. Anal. Calcd for $C_4H_{12}HgN_2S_2$: C, 13.62; H, 3.43; N, 7.94. Found: C, 13.66; H, 3.25; N, 7.98.

* To whom correspondence should be addressed
[†] Princeton University.
[‡] Northwestern University.

(1) Fleissner, G.; Reigle, M. D.; O'Halloran, T. V.; Spiro, T. G. *J. Am. Chem. Soc.* **1999**, *120*, 12690−12691.
(2) Watton, S. P.; Wright, J. G.; MacDonnell, F. M.; Bryson, J. W.; Sabat, M.; O'Halloran, T. V. *J. Am. Chem. Soc.* **1990**, *112*, 2824−2826.
(3) Church, W. B.; Guss, J. M.; Potter, J. J.; Freeman, H. C. *J. Biol. Chem.* **1986**, *261*, 234.
(4) Bryson, J. W. Ph.D. Thesis, Northwestern University, Evanston, IL, 1994.

10.1021/ic9810384 CCC: $18.00
Published on Web 07/02/1999

Ultraviolet Resonance Raman (UVRR) spectra were excited with the lines of an intracavity-doubled Ar^+ laser (Coherent Innova 300 FRED). The laser power was between 2 mW (229 nm) and 10 mW (257 nm excitation), measured at the source. A 135° backscattering geometry was used and a polarization scrambler was placed in front of the monochromator. The scattered light was collected using a 1.29 m single monochromator (SPEX 1269) equipped with a diode array detector (Princeton Instruments). Exposure of the sample to UV light was kept short (less than 1 min) and several scans (usually 20) with slightly changed vertical positions of the spinning sample tube were coadded. Nonresonant Raman spectra were excited with the 413 nm line of a Kr^+ laser (Coherent Innova 100-K3). The laser power was 23 mW. A holographic notch filter (Kaiser Optical Systems, HNF-413-1.0) was placed in front of the entrance slit of the single monochromator. For detection, a liquid nitrogen cooled CCD-detector was used (Princeton Instruments). The spectra are presented as recorded, without applying baseline correction or smoothing.

Raman intensities, expressed as cross sections, σ, were determined from the integrated intensity ratio, I_N/I_S, of the sample (N) and internal standard (S) vibrational bands by using

$$\sigma_N = \sigma_S(I_N/I_S)(C_S/C_N) \quad (1)$$

where C_S/C_N is the concentration ratio. Integrated band intensities were determined with the "curvefit" program of the Labcalc software (Galactic) using sums of Gaussian and Lorentzian band shapes, and including a linear baseline in the optimization process. For the 932 cm^{-1} band of ClO_4^- and the 918 cm^{-1} band of acetonitrile, absolute Raman cross sections have been determined for excitation in the visible as well as in the UV region.[5] These bands were used as internal standards to calculate absolute Raman cross sections of sample bands. Observed intensities in different regions of the Raman spectra may be differently affected by self-absorption. The influence of this effect was checked by calculating absolute Raman cross sections using two different acetonitrile bands at 918 and 380 cm^{-1} as internal standards. The results were the same within experimental error. UV−Vis absorption spectra were determined in a 1 mm quartz cuvette.

Far-IR spectra were recorded on a Nicolet 800 FTIR-spectrometer at 4 cm^{-1} resolution. The sample was placed on a polyethylene sheet (3M, 61-100-12). The Far-IR spectrum of the clean polyethylene sheet was digitally subtracted from the sample spectrum.

Geometry optimization and frequency calculations have been performed with the Gaussian 94 suite of programs for electronic structure calculation[6] at the Hartree−Fock level of theory with an effective core potential approximation (LanL2DZ, CEP-31G basis set[7]). The calculated Cartesian force constants were transformed to a set of internal coordinates as described in ref 8. The Hartree−Fock method typically overestimates force constants by 10−30% resulting in a 5−10% overestimation of vibrational frequencies.[8] This overestimation is rather systematic, usually depending on the type of bond involved, and can be corrected by scaling (scaling factors of approximately ~0.9 are often applied.)[9] Consistent with this expectation, the ν C−C internal ligand mode of $[Hg(SBu^t)_3]^-$, for example, is calculated at 877 cm^{-1} but observed at 820 cm^{-1} in the Raman spectrum (820/877 = 0.935). However, for modes, where the metal is directly involved, the expected overestimation of band positions is almost negligible. We expect that there is compensation because the effective core potential approximation for Hg leads to somewhat longer Hg−S bond lengths (e.g., for $[Hg(SBu^t)_3]^-$ 2.57 Å compared to 2.45 Å average bond length determined by X-ray crystallography).[10] Therefore, vibrational modes involving metal ligand modes are in agreement with experimental values, whereas internal ligand modes can be adjusted by scaling. Since vibrational calculations were performed mostly to assign metal ligand modes and experimental data are not sufficient to carry out scaling factors optimization, all calculated data are shown without scaling.

Table 1. Raman Bands and Calculated Mode Frequencies (cm^{-1}) and Descriptions for $Hg(SMe)_3^-$

calcd	expt Raman	symmetry	relative IR intensity[a]	mode description
41		E′	6.8	90% δ SHgS
50		E″	0	97% τ CSHgS
86		A″	37	90% δ oop HgS_3 10% t CSHgS
136		A′	0	89% δ HgSC
163	167	E′	15	75% δ HgSC 10% δ SHgS
268	282	A′	0	88% ν_s HgS
274		E′	100	85% ν_{as} HgS
705		E′	6.2	100% ν_{as} CS
706	700	A′	0	100% ν_s CS

[a] Relative IR intensities with respect to highest intensity.

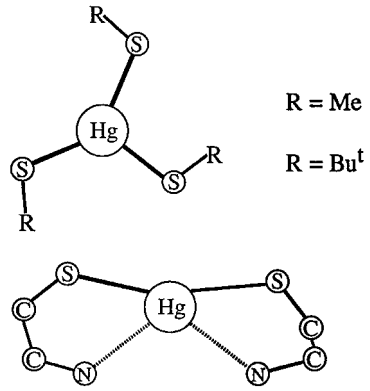

Figure 1. Schematic diagrams of Hg-thiolate complexes.

Results and Discussion

Where is the Hg−S stretch? $[Hg(SBu^t)_3]^-$ vs $[Hg(SMe)_3]^-$. $[Hg(SBu^t)_3]^-$ is an apt model complex for the trigonal $HgS(cys)_3$ coordination in the MerR regulatory protein.[11] Yet the Hg−S stretching vibration has been identified with RR bands having very different frequencies,[1] 282 cm^{-1} for MerR but 207 cm^{-1} for $[Hg(SBu^t)_3]^-$. Since the Hg−S bond distance is the same, 2.44 Å, for protein and model,[11] the difference in frequency was attributed to kinematic differences between the S(Cys) and SBu^t ligands. When the latter is replaced by SCH_3, the Raman band assigned to Hg−S stretching[4] is again at 282 cm^{-1}, just as in MerR.

To investigate the source of this difference we carried out ab initio calculations on $[Hg(SBu^t)_3]^-$ and $[Hg(SMe)_3]^-$, the results of which are given in Tables 1 and 2. Equilibrium structures were constrained to D_{3h} symmetry, and the calculated parameters are listed in Table 3, and shown in Figure 1; both complexes gave the same Hg−S distance, 2.58 Å. The data for $[Hg(SMe)_3]^-$ are sparse, but the vibrational pattern is straightforward. The three reported Raman bands,[12] 167, 282, and 700 cm^{-1}, are

(5) Dudik, J. M.; Johnson, C. R.; Asher, S. A. *J. Chem. Phys* **1985**, *82*, 1732−1740.
(6) Frisch, M. J.; Trucks, G. W.; Schlegel, H. B.; Gill, P. M. W.; Johnson, B. G.; Robb, M. A.; Chesseman, J. R.; Keith, T. A.; Petersson, G. A.; Montgomery, J. A.; Raghavachari, K.; Al-Laham, M. A.; Zakrzewski, V. G.; Ortiz, J. V.; Foresman, J. B.; Cioslowski, J.; Stefanov, B. B.; Nanayakkara, A.; Challacombe, M.; Peng, C. Y.; Ayala, P. Y.; Chen, W.; Wong, M. W.; Andres, J. L.; Replogle, E. S.; Gomperts, R.; Marin, R. L.; Fox, D. J.; Binkley, J. S.; Defrees, D. J.; Baker, J.; Stewart, J. P.; Head-Gordon, M.; Gonzalez, C.; Pople, J. A. *Gaussian 94*; Gaussian Inc.: Pittsburgh, PA, 1995.
(7) Stephens, W.; Basch, H.; Krauss, J. *J. Chem. Phys.* **1994**, *81*, 6026.
(8) Pulay, P.; Fogarasi, G.; Pongor, G.; Boggs, J. E.; Vargha, A. *J. Am. Chem. Soc.* **1983**, *105*, 7073.
(9) Rauhut, G.; Pulay, P. *J. Phys. Chem.* **1995**, *99*, 3093.
(10) (a) Canty, A. J.; Kishimoto, R.; Deacon, G. B.; Farquharson, G. J. *Inorg. Chim. Acta* **1976**, *20*, 161−166. (b) Jorgensen, C. K. *Prog. Inorg. Chem.* **1970**, *12*, 101.
(11) Utschig, L. M.; Wright, J. G.; O'Halloran, T. V. *Methods Enzymol.* **1993**, *226*, 71−97.
(12) Bowmaker, G. A.; Dance, I. G.; Dobson, B. C.; Rogers, D. A. *Aust. J. Chem.* **1984**, *37*, 1607−1618.

Table 2. IR[a] and Raman[b] Bands and Calculated Frequencies (cm^{-1}), and Descriptions for $Hg(SBu^t)_3^-$

calcd	expt Raman (IR)	symmetry	relative IR intensity	mode description[c]
50		E′	3.4	89% δ SHgS
65	(87)[a]	A″	32	100% δ_{oop} HgS_3
110	(110)[a]	E′	19	77% δ HgSC
110	(113)[a]	A′	1.2	84% δ HgSC
196	207[b]	A′	0	64% ν_s HgS 19% δ CCS
204	(208)[a]	E′	100	64% ν_{as} HgS 20% δ CCS
303		A″	0	98% τ HCCS/HCCC
303		E″	0	99% τ HCCS/HCCC
321	(308)[a]	A″	6.7	82% δ CCS 15% δ CCC
321		E″	0	82% δ CCS 15% δ CCC
338		A′	0	82% τ HCCS
339		E′	5.3	92% τ HCCS
352	341[b]	A′	0	41% δ CCS 31% δ CCC (3% ν HeS)
355	(337)[a]	E′	32	41% δ CCS 35% δ CCC (3% ν HgS)
415		A′	0	52% δ CCC/CCS 31% ν, CS
419	(380)[a]	E′	41	51% δ CCC/CCS 31% ν, CS
450		E″	0	74% δ CCC 14% δ CCS
450		A″	1.5	74% δ CCC 14% δ CCS
456		A′	0	47% δ CCC 39% δ CCS
457		E′	23	46% δ CCC 28% δ CCS
606		E′	70	50% ν_{as} Cs 26% δ CCC/CCS
608	588[b]	A′	0	49% ν, CS 26% δ CCC/CCS
877	820[b]	A′	0	80% ν CC
877	820[b]	E′	18	80% ν CC

[a] Reference 12. [b] Reference 1. [c] Only contributions $\geq$10% listed (except for bonds at 352 and 355 cm^{-1}).

Table 3. Selected Bond Distance (Å) and Angles (Deg) of the Hg-Thiolate Complexes

	$Hg(SMe)_3^-$	$Hg(SBut)_3^-$ [b]	$Hg(SCH_2CH_2NH_2)_2$[c]
		Bond Lengths	
HgS	(2.56)[a]	2.438, 2.451, 2.436 (2.57)[a]	2.361, 2.374 (2.47)[a]
HgN			2.66, 2.54 (2.71)[a]
CS	(1.89)[a]	(1.92)[a]	1.83, 1.81 (1.88)[a]
		Bond Angles	
HgSC	(105.11)[a]	(117.63)[a]	100.3, 98.6, (99.61)[a]
SHgS	(120.0)[a]	121.24, 120.85, 117.90 (120.00)[a]	161.1, (169.42)[a]
SCC		(114.18)[a]	115, 115, (114.46)[a]
NCC			112, 110, (111.75)[a]

[a] Calculated values are in parentheses. [b] Reference 2. [c] Reference 4.

Table 4. Raman and IR Bands and Calculated Mode Frequencies (cm^{-1}) and Descriptions for $Hg(SCH_2CH_2NH_2)_2$

calculated	expt Raman (IR)	symmetry	mode description[a]	Relative IR intensity
16		A	100% τ CSSC	3.3
45		B	74% Lin SHgSC, 15% τ HCSS/CCSS	2.5
52		A	50% Lin SHgSC, 48% τ HCSS/CCSS	1.7
91		B	85% τ HCSS/CCSS, 15% Lin SHgSC	0.04
93		A	48% Lin SHgSC, 52% τ HCSS/CCSS	2.2
120		A	100% δ HgSC	0.9
136	(153)	B	100% δ HgSC	5.4
210	217	A	66% τ HCCS/HCCN/NCCS, 13% ν HgS	0.7
230	(226)	B	90% τ HCCS/HCCN/NCCS, 10% ν HgS	3.3
273	273	A	33% HgS, 18% δ SCC, 9% δ NCC	0.4
286	(282)	B	42% δ SCC, 27% ν HgS, 20% δ NCC	7.2
337	339	A	41% δ SCC, 35% ν HgS, 21% δ NCC	0.7
357	(361)	B	60% ν HgS, 19% δ SCC, 14% δ NCC	19
425	(411)	B	66% τ HNCH/HNCC	4.1
436		A	55% τ HNCH/HNCC	8.7
525	(498)	B	49% δ NCC, 24% τ HNCH/HNCC	5.5
533	(510)	A	45% δ NCC, 35% τ HNCH/HNCC	7.1
680	658	A	80% ν CC	0.2
681	(660)	B	80% ν CS	3.8
916		A	33% δ HCC/HCS, 24% ν CN	6.3
916	(822)	B	31% δ HCC/HCS, 23% ν CN	68
958	(888)	B	57% δ_{oop} NH_2(C), 21% ν CC	100
960		A	59% δ_{oop} NH2(C), 20% ν CC	32

[a] Only contributions $\geq$10% listed.

readily assignable to HgSC bending, HgS stretching, and CS stretching coordinates, respectively. The symmetric (A′) and asymmetric (E′) HgS stretching modes are calculated to be only 6 cm^{-1} apart and would not have been detected separately. As required by symmetry, the IR intensity of A′ and E″ modes is zero (IR data are unavailable), while the Raman intensity is

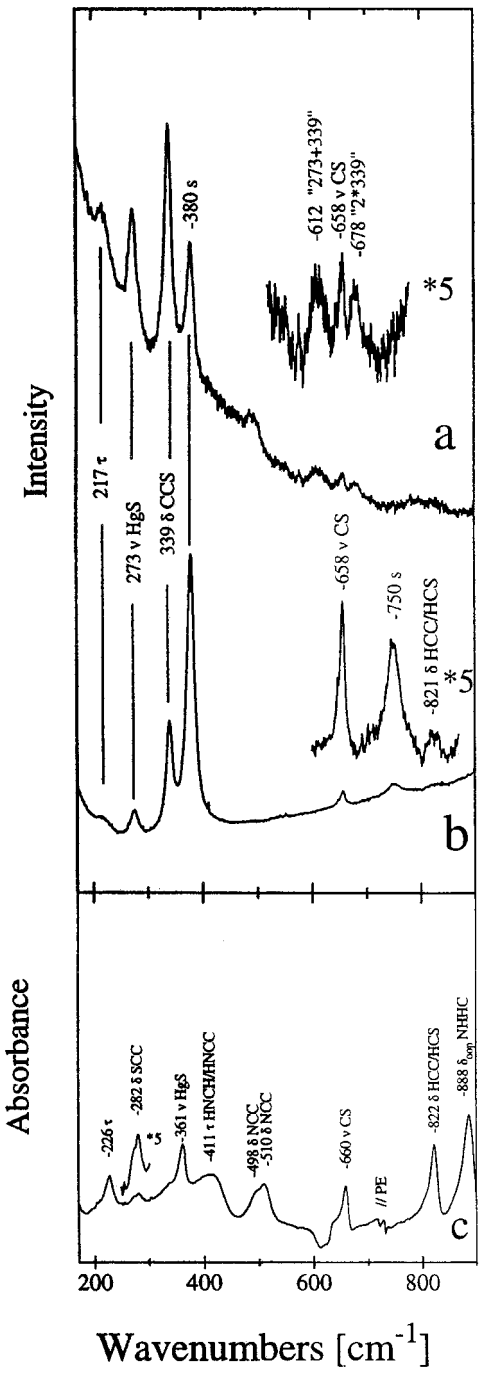

Figure 2. (a) UVRR (238 nm excitation, 15 mM concentration) and (b) Raman (413 nm excitation, 0.22 M conc.) spectra of $Hg(SCH_2CH_2NH_2)_2$ dissolved in acetonitrile; (c) far-IR spectrum of $Hg(SCH_2CH_2NH_2)_2$ in the solid state.

required to be zero for A″ modes (out-of-plane) and is expected to be low for E′ and E″ modes.

The vibrational pattern is less straightforward for $[Hg(SBu^t)_3]^-$ (Table 2), but substantial data are available from IR, Raman, and UVRR spectra. The IR bands[12] are all assignable to E′ and A″ modes with large calculated IR intensities, whereas modes with low calculated IR intensities are not observed. All the Raman bands are assignable to A′ modes.

The major kinematic change from $[Hg(SMe)_3]^-$ to $[Hg(SBu^t)_3]^-$ is that the CCC bending coordinate of the *tert*-butyl group interacts strongly with the C−S stretch, resulting in a mixed mode at 588 cm^{-1}, instead of an essentially pure C−S stretching mode at 706 cm^{-1} in $[Hg(SMe)_3]^-$. In turn the Hg−S stretch is heavily mixed with the CCS bending coordinate, resulting in a much lower frequency mode, at 207 cm^{-1}, in place of the essentially pure Hg−S stretch (282 cm^{-1}) of $[Hg(SMe)_3]^-$. This coordinate mixing occurs equally for the E′ and A′ Hg−S modes, which are calculated to be only 8 cm^{-1} apart; the assigned Raman and IR bands are essentially coincident. Consistent with its proposed assignment as an internal ligand mode,[1] the 341 cm^{-1} Raman band is calculated to be mostly CCS and CCC bending, with only a 3% contribution from Hg−S stretching; a corresponding IR mode is found at essentially the same frequency, 337 cm^{-1}. We note that a strong IR band at 110 cm^{-1}, previously assigned to SHgS bending,[12] is reassigned to HgSC bending; the calculated SHgS frequency is much lower, 50 cm^{-1}. The lowest observed IR band (87 cm^{-1}) may be the out-of-plane mode of the HgS_3 unit (calculated at 65 cm^{-1}).

Table 5. Mode Frequencies (cm^{-1}) and Descriptions for $Hg(SCH_2CH_2ND_2)_2$

calcd (expt) frequency	symmetry	mode description
203	A	68% τ HCCS/HCCN/NCCS 30% ν HgS
222	B	90% τ HCCS/HCCN/NCCS, 10% ν HgS
268 (266)	A	31% HgS, 19% δ SCC, 28% τ HCCS/HCCH/HCCN/NCCS
279	B	20% HgS, 40% d SCC, 24% d NCC
321	B	10% HgS, 72% τ DNCH/DNCC
323 (333)	A	29% HgS, 16% δ NCC, 37% τ DNCH/DNCC
343	A	12% HgS, 34% δ SCC, 40% τ DNCH/DNCC
357	B	58% HgS, 19% δ SCC, 11% δ NCC

Coordinate Mixing and the Chelate Effect in $Hg(SCH_2CH_2NH_2)_2$. The cysteamine complex is formally four-coordinate and pseudo-tetrahedral, but it can be more accurately described as a perturbed linear complex (SHgS angle of 161°), having secondary interactions of the amine groups with the Hg (Hg−N distance = 2.66 or 2.54 Å).[4]

However, the chelate rings have a pronounced influence on the low-frequency vibrations (Table 4). The Hg−S stretching coordinate is heavily mixed with SCC and NCC bending coordinates, and with torsional coordinates of the entire chelate rings, through no fewer than six normal modes between 360 and 210 cm^{-1}. Three of these are of B symmetry, with substantial calculated IR intensities, and three are of A symmetry, with low IR intensities. Raman intensities are expected to be higher for A than for B modes, and only A modes are subject to resonance Raman enhancement via the dominant Franck−Condon mechanism. These six modes are readily assigned in the observed vibrational spectra (Figure 2), to three IR bands, at 361, 282, and 226 cm^{-1}, and three Raman bands, at 339, 273, and 217 cm^{-1}. The ordering of the modes and their frequency agreement with the observed bands lends considerable confidence in the calculation. Moreover, the six modes are calculated to be altered substantially by N−H/D substitution (Table 5), because of the involvement of the CCN bending and DNCH torsion coordinates. The two strongest Raman bands do shift down significantly when $Hg(SCH_2CH_2NH_2)_2$ is dissolved in D_2O (Figure 4).

Additional infrared bands (Figure 2) are assignable to mixtures of torsions and bends of the chelate rings (411, 498, 510 cm^{-1}), to C−S stretching (660 cm^{-1}) and to mixtures of bending coordinates with C−N stretching (822 cm^{-1}) and C−C stretching (888 cm^{-1}). C−S stretching also gives rise to a Raman band at essentially the IR frequency (658 cm^{-1}), as predicted by the calculation.

Resonance Enhancement. The 339, 273, and 217 cm^{-1} Raman bands of $Hg(SCH_2CH_2NH_2)_2$ are all enhanced with UV excitation, as can be seen from the higher intensity, relative to

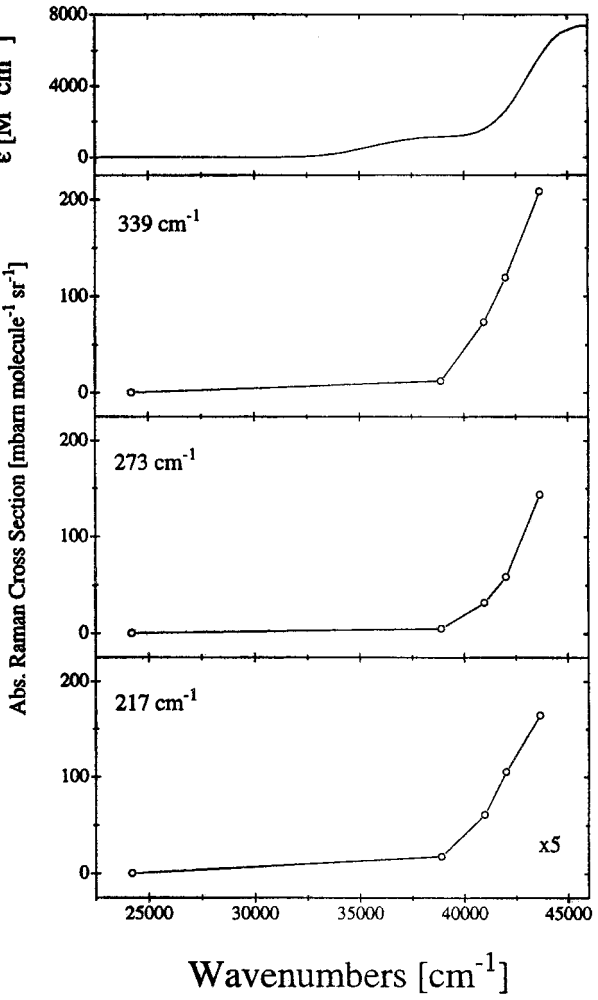

Figure 3. UV absorption spectrum of $Hg(SCH_2CH_2NH_2)_2$ dissolved in acetonitrile (top panel) and absolute Raman intensities for bands at 339, 273, and 217 cm^{-1} (lower panels).

the 380 cm^{-1} solvent band, with 238 than with 413 nm excitation (Figure 2). The 339 and 273 cm^{-1} RR bands are sufficiently enhanced to produce detectable combination and overtone bands, bracketing the weakly enhanced 658 cm^{-1} C−S stretch (Figure 2). When the Raman cross-sections are plotted at a series of wavelengths (Figure 3), it can be seen that the enhancement tracks the major UV absorption band, maximizing at ∼45 000†cm^{-1}. This band is assigned to S→Hg charge transfer. A weaker electronic transition, which produces a ∼38 000 cm^{-1} absorption, is without discernible influence on the RR enhancement.

The Hg−S contribution to the three RR modes increases in the order 217 (13%) < 273 (33%) < 337 (35%) cm^{-1}, as does the Raman cross-section (Table 6). However, the 337 cm^{-1} band is 30% stronger than the 273 cm^{-1} band, despite having only 2% higher Hg−S contribution. We infer that the SCC bending coordinate, which is the dominant contributor to the 337 cm^{-1} mode, is also displaced significantly in the S→Hg excited state, along with the Hg−S stretch. A similar effect is evident in the $[Hg(SBu^t)_3]^-$ RR spectrum[1], since the 341 cm^{-1} is half as strong as the 207 cm^{-1} band, even though the Hg−S contributions are 3 and 64%, respectively (Table 2). The SCC bending coordinate contributes 41% to the 341 cm^{-1} mode, and must account for most of its enhancement. Displacement along the SCC bending coordinate implies that the S→Hg charge transfer expands the SCC bond angle, a plausible consequence of increased hyperconjugation in the S−C bond.

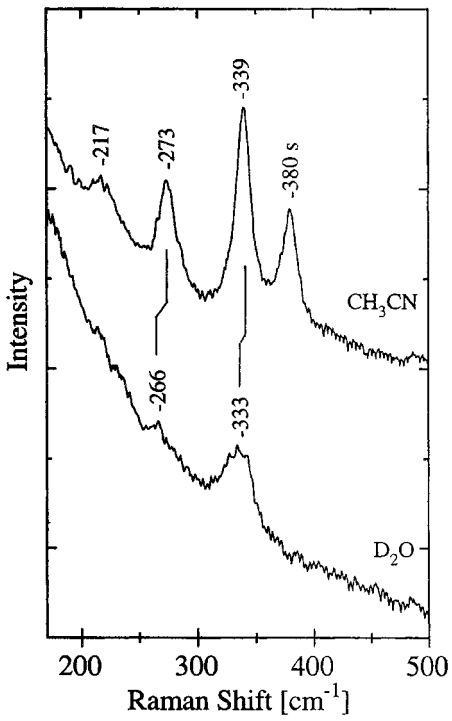

Figure 4. UVRR spectra of $Hg(SCH_2CH_2NH_2)_2$ dissolved in acetonitrile (top) and in D_2O (bottom) at 238 nm excitation.

Table 6. Raman Cross-Sections[a] for $Hg(SCH_2CH_2NH_2)_2$ in Acetonitrile

wavelength (nm)	ϵ (M^{-1} cm^{-1})	σ_{217}	σ_{273}	σ_{339}
229	5800	144	165	208
238	2800	59	105	119
244	1500	32	60	73
257	1100	5	17	12
413[b]	100	0.06	0.1	0.2

[a] Expressed in units of cross-section, [millibarns/(molecule steradian)], 1 barn = 10^{-24} cm^2. [b] Kr^+ (Coherent), Spex 1877 triple spectrometer equipped with an intensified diode array detector (Princeton Instruments).

Interestingly, the aggregate cross-sections for $Hg(SCH_2CH_2NH_2)_2$ (Table 6) are roughly three times those observed[1] for $[Hg(SBu^t)_3]^-$.

The coordinate mixing pattern for $Hg(SCH_2CH_2NH_2)_2$ is similar to that encountered for type1 Cu proteins, which likewise show RR enhancement of multiple low-frequency bands in resonance with the S→Cu charge transfer transition.[14] Isotopic substitution in azurin[22] and plastocyanin[21] has revealed mixing of the Cu−S stretch with several deformation modes of the cysteine side chain. It seems likely that the mixing of deforma-

(13) Spiro, T. G.; Stein, P. *Annu. Rev. Phys. Chem.* **1977**, *28*, 501−521.
(14) Woodruff, W. H.; Dyer, R. B.; Schoonover, J. R. In *Biological Applications of Raman Spectroscopy*; Spiro, T. G., Ed.; Wiley-Interscience: New York, 1987; Vol. 3, Chapter 9.
(15) O'Halloran, T. V.; Frantz, B.; Shin, M. K.; Ralston, D. M.; Wright, J. G. *Cell* **1989**, *56*,119−129.
(16) Wright, J. G.; Natan, M. J.; MacDonnell, F. M.; Ralston, D. M.; O'Halloran, T. V. In *Progress in Inorganic Chemistry*; Lippard, S. J., Ed.; Wiley: New York, 1990; pp 323−412.
(17) Ueyama, N.; Nakata, M.; Nakamura, A. *Bull. Chem. Soc. Jpn.* **1985**, *58*, 464−469.
(18) Yachandra, V. K.; Hare, J.; Moura, I.; Spiro, T. G. *J. Am. Chem. Soc.* **1983**, *105*, 6455−6461.
(19) Sugeta, H. *Spectrochim. Acta, Part A* 1975, *31A*, 1729.
(20) Qiu, D.; Kilpatrick, L.; Kitajima, N.; Spiro, T. G. *J. Am. Chem. Soc.* **1994**, *116*, 2585−2590.
(21) Nestor, L.; Larrabee, J. A.; Woolery, G.; Reinhammar, B.; Spiro, T. G. *Biochemistry* **1984**, *23*, 1084−1093.

tion and M−S stretching coordinates is facilitated by the ligand rigidity, which is provided by chelation in $Hg(SCH_2CH_2NH_2)_2$, and by the connectivity constraints of the polypeptide chain in the Cu proteins. The more extensive coordinate mixing displayed by the proteins probably results from the coplanarity of the CuSCCN atomic framework, which has been observed in all type 1 Cu structures.[20]

Conclusions

Coordinate mixing is responsible for substantial variability in vibrational band frequencies between Hg−S proteins and models. In $[Hg(SBu^t)_3]^-$, the modes with predominant Hg−S contributions are strongly lowered in frequency by interaction with the SCC bending coordinate, which in turn results from mixing of the CCC umbrella coordinates with the C−S stretch. This effect is not seen if two or more of the *tert*-butyl methyl groups are replaced by H, so that Hg-MerR and $[Hg(SMe)_3]^-$ both show Hg−S Raman bands at 282 cm^{-1}, much higher than $[Hg(SBu^t)_3]^-$ (207 cm^{-1}). A more complex pattern is found in $Hg(SCH_2CH_2NH_2)_2$, for which the Hg−S coordinate is mixed with ligand deformations in six different normal modes, three of which are enhanced in the UVRR spectrum. The additional mixing is attributed to ligand rigidity resulting from the cysteamine chelate rings. This effect is reminiscent of the complex mixing pattern seen in the RR spectra of type 1 Cu proteins, in which the cysteine ligand is likewise rigid, and in addition is coplanar with the C−S bond.

Resonance enhancement via the S→Hg charge transfer transitions is evident for modes having substantial SCC bending, as well as Hg−S stretching contributions, implying that the SCC bond angles expand while the Hg−S bonds stretch in the excited state.

Acknowledgment. This work was supported by NIH grants GM 13498 (to T.G.S.) and GM 38784 (to T.V.O.).

IC9810384

(22) Han, J.; Adman, E. T.; Beppu, T.; Codd, R.; Freeman, H. C.; Huq, L.; Loehr, T. M.; Sanders-Loehr, J. *Biochemistry* **1991**, *30*, 10904−10913.